Scanning Electrochemical Microscopy. 9. Theory and Application of the Feedback Mode to the Measurement of Following Chemical Reaction Rates in Electrode Processes

Patrick R. Unwin and Allen J. Bard*

Department of Chemistry, The University of Texas at Austin, Austin, Texas 78712
(Received: February 12, 1991)

The use of the scanning electrochemical microscope (SECM), in both the steady-state and chronoamperometric feedback modes, is proposed as a new method for measuring the kinetics of following chemical reactions in electrode processes. Particular attention is given to the E_rC_i mechanistic case (first-order irreversible chemical step following reversible electron transfer). Theory for the problem, relating the SECM feedback current to the tip–substrate distance, tip electrode radius, and rate constant for the chemical step, is developed numerically by using the alternating-direction implicit finite-difference scheme. The theoretical results demonstrate that both the chronoamperometric and steady-state feedback modes are sensitive techniques for accurate kinetic determinations, and that homogeneous chemical rate constants in excess of 2×10^4 s^{-1} should be accessible to measurement with current SECM technology. The theoretical predictions are verified experimentally with the measurement of the rate of deamination, in aqueous basic solution (pH 10.2–12.4), of oxidized *N,N*-dimethyl-*p*-phenylenediamine, produced at a platinum electrode.

Introduction

Recent papers from this group have described the principles of scanning electrochemical microscopy (SECM)[1,2] and the theory of the steady-state[3] and chronoamperometric[4] feedback modes. A diversity of applications have been demonstrated involving both the characterization[5-8] and modification[9-14] of surfaces. In addition, the technique can be used in the feedback mode, with conducting substrates, for electrochemical kinetic investigations.[4,15] In this mode, the tip ultramicroelectrode, held at a potential for the diffusion-controlled electrolysis of a target species in solution, experiences positive diffusional feedback when positioned close (within a distance of about 10 electrode radii) to a conductor, poised at a potential such that the direction of the tip electrode reaction is reversed on its surface (see Figure 1a). The small electrode–substrate separations which may be realized with SECM (down to fractions of a micrometer[15,16]), promote high rates of (steady-state) diffusion to the tip, making this electrode configuration attractive for studying the rates of fast heterogeneous electron transfer and, as discussed in this paper, coupled homogeneous chemical reactions in the gap region.

It was demonstrated in a previous paper that heterogeneous rate constants in excess of 1 cm s^{-1} could be distinguished by using the feedback SECM approach.[15] In this paper we extend the application of SECM as an electrochemical kinetic technique by considering the study of the rates of homogeneous chemical reactions coupled to electron transfer. Particular attention is given to the case of a first-order chemical step following a reversible electron transfer, i.e., the E_rC_i mechanism[17] (written here as an oxidation process)

electrode: $$R - ne \rightarrow O \quad (E_r) \tag{1}$$

solution: $$O \xrightarrow{k_c} P \quad (C_i) \tag{2}$$

where n is the number of electrons transferred per redox event and k_c is the rate constant for the homogeneous chemical reaction.

The principle behind the use of feedback SECM to study the kinetics of the chemical step is illustrated schematically in Figure 1b. The aim is to set up a competition between, on the one hand, the diffusion of O from the tip to the substrate (with subsequent regeneration of R and consequent feedback) and, on the other, the decomposition of O to the product, P. The kinetics of the chemical step are probed by varying the tip–substrate distance, and thus the diffusion time of O to the conductor, and measuring the tip current, i_T. When the tip–substrate diffusion time, of the order of d^2/D (where d is the tip–substrate distance and D the diffusion coefficient), is short compared to the lifetime of O, of the order of $1/k_c$, i_T will attain values expected for conductive substrate feedback in the absence of homogeneous kinetics. In the fast kinetic limit, the tip response will be similar to that for an insulating substrate, since little O will survive the passage across the gap to the substrate for regeneration to R. Thus it is convenient to consider the observed behavior in terms of the dimensionless parameter d^2k_c/D:

$d^2k_c/D \gg 1$, SECM insulating substrate behavior

$d^2k_c/D \ll 1$, SECM conductive substrate behavior

$d^2k_c/D \approx 1$, kinetic measurements possible

It is anticipated that the great difference in i_T, for feedback from conducting and insulating substrates (up to 100-fold under steady-state conditions[3]), should make this technique extremely sensitive for the measurement of intermediate kinetic cases.

A vast number of electrochemical methods have previously been proposed for kinetic studies of the E_rC_i mechanism.[18-37] Reversal

(1) Bard, A. J.; Fan, F.-R. R.; Kwak, J.; Lev, O. *Anal. Chem.* **1989**, *61*, 132.
(2) Bard, A. J.; Denault, G.; Lee, C.; Mandler, D.; Wipf, D. O. *Acc. Chem. Res.* **1990**, *23*, 357.
(3) Kwak, J.; Bard, A. J. *Anal. Chem.* **1989**, *61*, 1221.
(4) Bard, A. J.; Denault, G.; Dornblaser, B. C.; Friesner, R. A.; Tuckerman, L. S. *Anal. Chem.* **1991**, *63*, 1282.
(5) Kwak, J.; Bard, A. J. *Anal. Chem.* **1989**, *61*, 1794.
(6) Lee, C.; Bard, A. J. *Anal. Chem.* **1990**, *62*, 1906.
(7) Kwak, J.; Lee, C.; Bard, A. J. *J. Electrochem. Soc.* **1990**, *137*, 1481.
(8) Lee, C.; Kwak, J.; Bard, A. J. *Proc. Natl. Acad. Sci. U.S.A.* **1990**, *87*, 1740.
(9) Craston, D. H.; Lin, C. W.; Bard, A. J. *J. Electrochem. Soc.* **1988**, *135*, 785.
(10) Hüsser, O. E.; Craston, D. H.; Bard, A. J. *J. Vac. Sci. Technol. B* **1988**, *6*, 1873.
(11) Hüsser, O. E.; Craston, D. H.; Bard, A. J. *J. Electrochem. Soc.* **1989**, *136*, 3222.
(12) Wuu, T.-M.; Fan, F.-R. F.; Bard, A. J. *J. Electrochem. Soc.* **1989**, *136*, 885.
(13) Mandler, D.; Bard, A. J. *J. Electrochem. Soc.* (a) **1990**, *137*, 1079; (b) **1989**, *136*, 3143; (c) **1990**, *137*, 2468.
(14) Mandler, D.; Bard, A. J. *Langmuir* **1990**, *6*, 1489.
(15) Wipf, D. O.; Bard, A. J. *J. Electrochem. Soc.* **1991**, *138*, 469.
(16) Lee, C.; Miller, C. J.; Bard, A. J. *Anal. Chem.* **1991**, *63*, 78.
(17) Bard, A. J.; Faulkner, L. R. *Electrochemical Methods*; Wiley: New York, 1980.
(18) Nicholson, R. S.; Shain, I. *Anal. Chem.* **1964**, *36*, 706.
(19) Schwarz, W. M.; Shain, I. *J. Phys. Chem.* **1965**, *69*, 30.

0022-3654/91/2095-7814$02.50/0

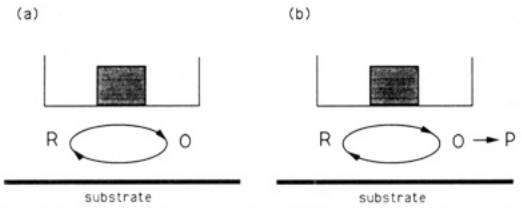

Figure 1. Principles of the operation of the scanning electrochemical microscope in the feedback mode, over a conductive substrate, for (a) a simple redox couple O/R and (b) the EC mechanism, where the species O decomposes in solution while diffusing from the tip to the substrate.

techniques, such as cyclic voltammetry,[18] double-potential-step chronoamperometry[19] and chronocoulometry,[20] and various current reversal[21,22] and pulse[23] methods have been shown to be particularly powerful, as have collection efficiency measurements at "double electrodes" such as the rotating ring-disk electrode,[24] dual electrode in a thin-layer cell (TLC),[25] double channel or tubular electrode,[26] interdigitated channel array electrode,[27] and paired microband electrode.[28] The basis of these methods is to collect the fraction of species O which remains at a prescribed time after its electrochemical generation, either by reversing the direction of the initial potential or current perturbation at the electrode, or by employing a second electrode to collect O. Even in the absence of kinetic complications, however, only a fraction of O is generally collected, with a large portion of the species being lost to the solution through diffusion. This is to be contrasted with the situation in the feedback SECM approach, outlined above, where the redox cycling of O and R between the tip and substrate leads to large currents at the tip electrode in comparison to the steady-state current in the absence of a substrate. In this sense the SECM is similar to a dual electrode ultra-thin-layer cell,[38] but the SECM has the advantage that continuous diffusion of new material into the gap makes steady-state measurements possible on reactions in which the reactants are consumed with time (such as in the E_rC_i mechanism).

In this paper we consider the application of both steady-state and potential-step chronoamperometric feedback at the SECM to investigate the problem set out above. Theory is developed numerically using the alternating-direction implicit (ADI) finite-difference scheme, which has been shown to be an efficient method for solving time-dependent two-dimensional problems.[39-41] Working curves for both the steady-state and transient approaches are calculated, and the range of rate constants accessible to measurement is defined. The theoretical predictions are tested on the standard E_rC_i process of the deamination of oxidized *N,N*-dimethyl-*p*-phenylenediamine[26,35,42] electrogenerated in aqueous basic solution at a platinum electrode.

Theory

Formulation of the Problem. For the E_rC_i mechanism, eqs 1 and 2, the diffusion equations for species R and O appropriate to the SECM geometry, in cylindrical coordinates, are of the form

$$\frac{\partial c_R}{\partial t} = D_R\left[\frac{\partial^2 c_R}{\partial r^2} + \frac{1}{r}\frac{\partial c_R}{\partial r} + \frac{\partial^2 c_R}{\partial z^2}\right] \tag{3}$$

$$\frac{\partial c_O}{\partial t} = D_O\left[\frac{\partial^2 c_O}{\partial r^2} + \frac{1}{r}\frac{\partial c_O}{\partial r} + \frac{\partial^2 c_O}{\partial z^2}\right] - k_c c_O \tag{4}$$

where r and z are respectively the coordinates in the directions radial and normal to the electrode surface; D_i and c_i are the diffusion coefficient and concentration of the species i (i = O, R), and t is time. For the chronoamperometric feedback experiment, it is assumed that only R is present in solution at the bulk concentration c_R^* (over all space) prior to the potential step and so the initial condition is

$$t = 0: \qquad c_R = c_R^*, \quad c_O = 0 \tag{5}$$

Subsequently the tip electrode potential is stepped to a value for the diffusion-controlled oxidation of R, while the substrate potential is maintained at a value so that the reverse reaction takes place at a diffusion-controlled rate on its surface. O and R are assumed to be inert on the insulating (glass) sheath surrounding the tip microdisk electrode, and to remain at their bulk concentration values (zero and c_R^*, respectively) across all of the gap, beyond the radial edge of the tip–substrate domain. Additionally, the axisymmetric geometry implies that there is zero radial flux of R or O at $r = 0$, $0 < z < d$. The boundary conditions for this situation are therefore

$$z = 0,\ 0 \le r \le a \text{ (tip electrode)}: \quad c_R = 0,\ D_R\frac{\partial c_R}{\partial z} = -D_O\frac{\partial c_O}{\partial z} \tag{6}$$

$$z = 0,\ a \le r \le r_{glass} \text{ (glass sheath)}: \quad D_R\frac{\partial c_R}{\partial z} = D_O\frac{\partial c_O}{\partial z} = 0 \tag{7}$$

$$z = d,\ 0 \le r \le r_{glass} \text{ (substrate)}: \quad c_O = 0,\ D_R\frac{\partial c_R}{\partial z} = -D_O\frac{\partial c_O}{\partial z} \tag{8}$$

$$r \ge r_{glass},\ 0 \le z \le d \text{ (radial edge of the tip–substrate domain)}: \quad c_R = c_R^*,\ c_O = 0 \tag{9}$$

$$r = 0,\ 0 < z < d \text{ (axis of symmetry)}: \quad D_R\frac{\partial c_R}{\partial r} = D_O\frac{\partial c_O}{\partial r} = 0 \tag{10}$$

The theory of diffusion to ultramicroelectrodes,[43] and previous SECM steady-state feedback theory,[3] indicate that the eq 9 is valid

(20) Childs, W. V.; Maloy, J. T.; Keszthelyi, C. P.; Bard, A. J. *J. Electrochem. Soc.* **1971**, *118*, 874.
(21) Testa, A. C.; Reinmuth, W. H. *Anal. Chem.* **1960**, *32*, 1512.
(22) Herman, H. B.; Bard, A. J. *Anal. Chem.* **1964**, *36*, 510.
(23) Mizota, H.; Aoyagui, S. *J. Electroanal. Chem. Interfacial Electrochem.* **1978**, *87*, 165.
(24) Albery, W. J.; Hitchman, M. L. *Ring Disc Electrodes*; Clarendon Press: Oxford, U.K., 1971.
(25) Anderson, L. B.; Reilly, C. N. *J. Electroanal. Chem. Interfacial Electrochem.* **1965**, *10*, 538.
(26) Aoki, K.; Matsuda, H. *J. Electroanal. Chem. Interfacial Electrochem.* **1978**, *94*, 157.
(27) Ou, T. Y.; Moldoveanu, S.; Anderson, J. L. *J. Electroanal. Chem. Interfacial Electrochem.* **1988**, *247*, 1.
(28) Varco Shea, T.; Bard, A. J. *Anal. Chem.* **1987**, *59*, 2101.
(29) Testa, A. C.; Reinmuth, W. H. *Anal. Chem.* **1960**, *32*, 1518.
(30) McCord, T. G.; Hung, H. L.; Smith, D. E. *J. Electroanal. Chem. Interfacial Electrochem.* **1969**, *21*, 5.
(31) McCord, T. G.; Smith, D. E. *Anal. Chem.* **1969**, *41*, 1423.
(32) O'Dea, J. J.; Osteryoung, J. *Anal. Chem.* **1981**, *53*, 695.
(33) Bilewicz, R.; Wikiel, K.; Osteryoung, R.; Osteryoung, J. *Anal. Chem.* **1989**, *61*, 965.
(34) Saveant, J. M.; Tessier, D. *J. Electroanal. Chem. Interfacial Electrochem.* **1975**, *61*, 251.
(35) Tong, L. K. J.; Liang, K.; Ruby, W. R. *J. Electroanal. Chem. Interfacial Electrochem.* **1967**, *13*, 245.
(36) Coles, B. A.; Compton, R. G. *J. Electroanal. Chem. Interfacial Electrochem.* **1981**, *127*, 37.
(37) Kim, M.-H. *J. Electrochem. Soc.* **1990**, *137*, 3815.
(38) Davis, J. M.; Fan, F.-R. F.; Bard, A. J. *J. Electroanal. Chem. Interfacial Electrochem.* **1987**, *238*, 9.
(39) Peaceman, D. W.; Rachford, H. H. *J. Soc. Ind. Appl. Math.* **1955**, *3*, 28.
(40) Lapidus, L.; Pinder, G. F. *Numerical Solution of Partial Differential Equations in Science and Engineering*; Wiley: New York, 1982.
(41) Ames, W. F. *Numerical Methods of Partial Differential Equations*; Wiley: New York, 1977.
(42) Tong, L. K. J. *J. Phys. Chem.* **1954**, *58*, 1090.
(43) (a) Wightman, R. M. *Science* **1988**, *240*, 415. (b) Wightman, R. M.; Wipf, D. O. In *Electroanalytical Chemistry*; Bard, A. J., Ed.; Marcel Dekker: New York, 1988; Vol. 15, p 267.

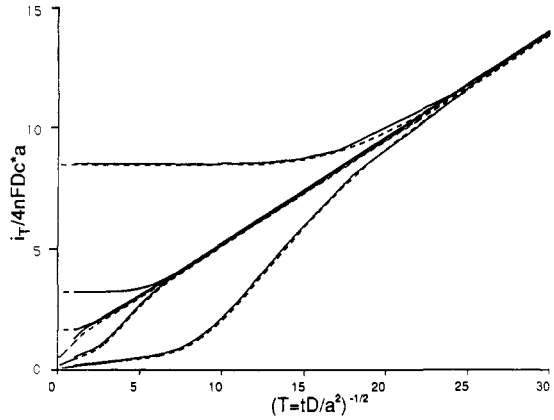

Figure 2. Simulated SECM current transients displayed as a function of the inverse square root of time. The upper curves correspond to a conductive substrate [log (d/a) = −1.0, −0.5, 0.0 starting with the top curve] and the bottom curves to an insulating substrate [log (d/a) = −1.0, −0.5, 0.0 starting with the lowest curve]. The results of the ADI method (---) are observed to be in good agreement with those obtained with the Krylov integration technique (—).[4]

for RG = $r_{glass}/a \geq 10$. For tip electrodes characterized by smaller ratios, consideration of diffusion at $r > r_{glass}$ may be required.

To obtain general solutions, the problem is cast into dimensionless form through the introduction of the following variables:[3]

$$R = r/a \tag{11}$$

$$Z = z/a \tag{12}$$

$$C_i = c_i/c_R^* \tag{13}$$

$$T = tD/a^2 \tag{14}$$

$$K = k_c a^2/D \tag{15}$$

The last two equations imply that only the case where $D = D_R = D_O$ will be considered, for simplicity. The effect of unequal diffusion coefficients of participating species in SECM will be considered later.

The aim of the calculations is to determine the tip current response as a function of time, T, the former quantity being given by

$$i_T = nFD\int_0^a 2\pi r(\partial c_R/\partial z)_{z=0}\,dr \tag{16}$$

where F is the Faraday. In dimensionless form this becomes

$$(i_T/i_{T,\infty}) = (\pi/2)\int_0^1 (\partial C_R/\partial Z)_{Z=0} R\,\partial R \tag{17}$$

where the denominator on the left-hand side of the above equation denotes the steady-state current at a simple microdisk electrode:[43,44]

$$i_{T,\infty} = 4nFDc_R^*a \tag{18}$$

Method of Solution. The problem as set out above was solved numerically by using the alternating-direction implicit (ADI) finite-difference method. Since its introduction by Peaceman and Rachford,[39] this technique has found widespread application as an efficient method for solving multidimensional transient problems in a variety of fields,[40,41] and has recently been successfully applied to electrochemical microelectrode problems.[45-47] A complete discussion of the method can be found in the original literature;[39] an outline of the application of the ADI method to the SECM problem considered here is given in the Appendix.

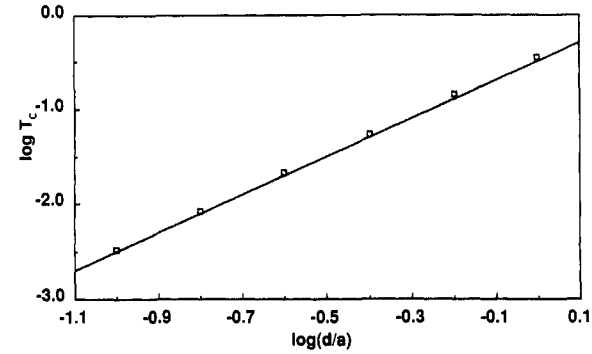

Figure 3. The variation of the dimensionless critical time, T_c ($=t_cD/a^2$), with the ratio d/a for SECM feedback with a conductive substrate (□). The straight line shows the equivalent behavior derived for a dual-electrode thin-layer cell (eq 19).

Theoretical Results and Discussion

Preliminary Calculations. In order to check the accuracy of the ADI method, the chronoamperometric characteristics for simple feedback over insulating and conducting substrates were evaluated, since these cases have been considered previously using an integrator based on a Krylov algorithm.[4] Typical results, presented as $i_T/4nFDac^*$ vs $T^{-1/2}$ ($T^{-1/2}$ being suggested by the theory for diffusion-controlled reactions at planar or ultramicroelectrodes[17]) for different ratios of d/a, are shown in Figure 2. A value of RG = 10 was used for these, and all subsequent, calculations. The results of the two independent methods are seen to be in good agreement, confirming the validity of using the ADI method for SECM time-dependent problems. In addition, the steady-state currents, derived from the data in the limit of long time, were found to be close to those obtained previously using the finite element method.[3]

The form of the chronoamperometric feedback characteristics for SECM was discussed in detail in a previous paper.[4] For the purposes of the discussion which follows, it is necessary to reintroduce the concept of a critical diffusion time, T_c, for feedback from a conductor.[4] T_c is essentially a measure of the time required for the tip to sense the presence of the substrate in the chronoamperometric mode, of the order of twice the tip–substrate diffusion time for a conductive substrate. For a particular d/a ratio, T_c is conveniently defined as the time at which a simple ultramicrodisk electrode attains an equivalent current to that resulting from steady-state feedback to an identical disk in the SECM configuration (see Figure 5 of ref 4 for further details). A plot of T_c as a function of d/a, determined from simulated transients, such as those in Figure 2, is shown in Figure 3. It is important to note that for the practical values of d/a considered here, edge effects arising from radial diffusion are negligible at T_c, as evidenced by the fact that the calculated T_c–d/a behavior is very close to that predicted for the analogous thin-layer cell situation in which only one-dimensional diffuson (normal to the electrode) needs to be considered:[4]

$$\log T_c = 2\log(d/a) - \log\pi \tag{19}$$

Chronoamperometric Characteristics for the EC Mechanism. Typical calculated chronoamperometric behavior for the EC mechanism in the feedback mode for two ratios of d/a and different values of K are shown in Figure 4a,b. The calculated behavior in the absence of the chemical step above both conducting and insulating substrates is also shown for comparison with the kinetic characteristics. At short times (large $T^{-1/2}$), the i_T response is independent of both d/a and K since the diffusion field around the electrode is small compared to the size of the gap and thus the electrode displays the behavior predicted for a simple ultramicrodisk electrode:[48]

$$\frac{i_T(T)}{i_T(T\to\infty)} = 0.7854 + 0.4431T^{-1/2} + 0.2146\exp(-0.3911T^{-1/2}) \tag{20}$$

(44) Saito, Y. *Rev. Polarogr. Jpn.* **1968**, *15*, 177.
(45) (a) Heinze, J. *J. Electroanal. Chem. Interfacial Electrochem.* **1981**, *124*, 73. (b) Heinze, J. *Ber. Bunsen-Ges. Phys. Chem.* **1981**, *85*, 1096. (c) Heinze, J.; Storzbach, M. *Ber. Bunsen-Ges. Phys. Chem.* **1986**, *90*, 1043.
(46) Taylor, G.; Girault, H. H.; McAleer, J. *J. Electroanal. Chem. Interfacial Electrochem.* **1990**, *293*, 19.
(47) Gavaghan, D. J.; Rollet, J. S. *J. Electroanal. Chem. Interfacial Electrochem.* **1990**, *295*, 1.

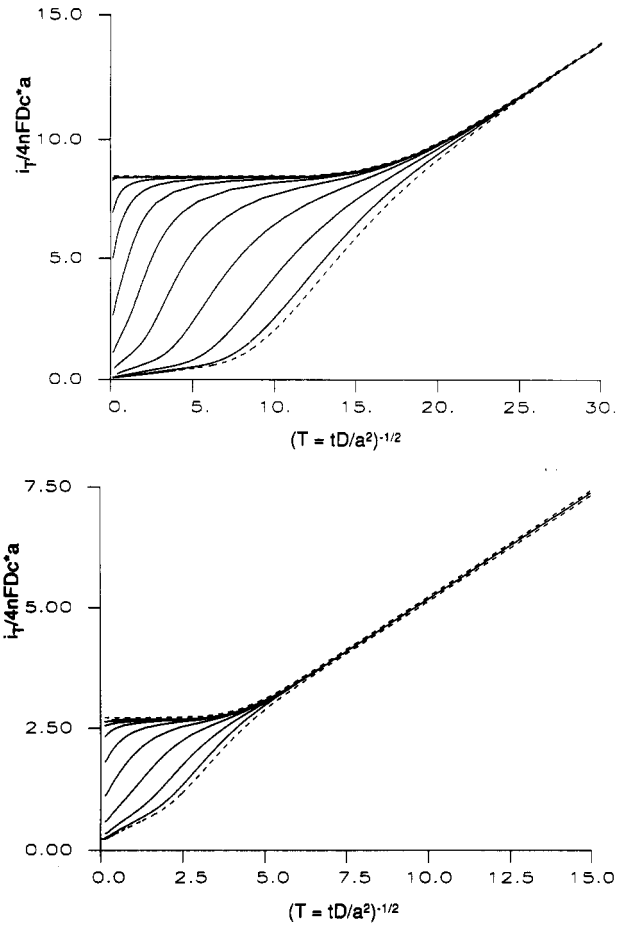

Figure 4. Simulated SECM feedback current transients for an E_rC_i process, displayed as $T^{-1/2}$, for log (d/a) = (a, top) −1.0 and (b, bottom) −0.4. The upper and lower dashed curves in each diagram correspond, respectively, to the kinetically uncomplicated feedback behavior from conducting and insulating substrates. The curves lying between these two extremes represent (a) log K = −2.0 (upper solid curve), −1.5, −0.5, 0.0, 0.5, 1.0, 1.5, 2.0, 2.5, 3.0 (lower solid curve) and (b) log K = −2.2 (upper solid curve), −1.7, −1.2, −0.7, −0.2, 0.3, 0.8, 1.3, 1.8 (lower solid curve).

Once the tip electrode senses the substrate, the subsequent current–time characteristics depend upon the size of K. For the smallest values considered in Figure 4, the behavior closely follows that expected for diffusional feedback from a conducting substrate. Under these conditions the reaction layer,[17] z_R, in which R exists (considering diffusion in the z direction only)

$$\frac{z_R}{d} = \frac{a(K)^{-1/2}}{d} \tag{21}$$

is large compared to the size of the gap and thus there is little decomposition of O in its transit to the substrate. For intermediate values of K (for a given d/a ratio), the current–time characteristics initially follow the behavior for feedback from a conductive substrate without following kinetic complications, i.e., a rapid quasi-steady-state current is attained, as evidenced by the plateau regions in the i_T–$T^{-1/2}$ plots. Under these conditions, the rates of diffusion in the SECM are sufficiently rapid to outrun the following chemical kinetics. At times comparable to the lifetime of O, deviation from pure conductor feedback behavior is observed, as the homogeneous chemical process consumes this species. Clearly, the larger the value of K, the shorter the time at which the deviation occurs and the smaller the final steady-state value of i_T. In the limit $K \to \infty$, the picture is essentially that of feedback from an insulator; the reaction layer thickness (and lifetime) of O tends to zero and thus a regime of negative feedback is observed. In order to emphasize the length of time required for the establishment of the true (final) steady-state in SECM chronoamperometry, Figure 5 shows the long-time behavior of the data in Figure 3 in greater detail. It can be seen that normalized times in excess of 100 are necessary to achieve steady-state conditions, which must be taken into account when making experimental measurements of the steady-state diffusion-limited tip current as a function of tip–substrate distance.

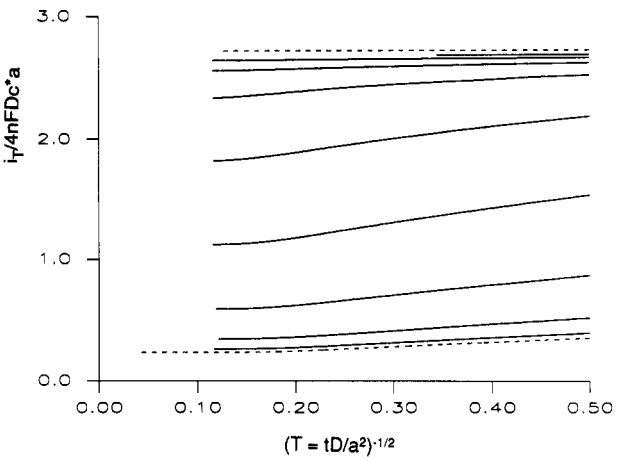

Figure 5. The long-time behavior of the data in Figure 4b.

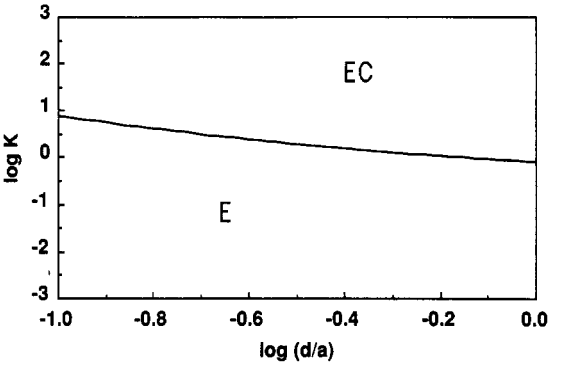

Figure 6. Zone diagram for the i_T–T characteristics, up to $T = (1.1)^{-2}(2T_c)$, indicating the kinetic domains in which the following chemical reaction (i) has essentially no effect on the transient behavior (indicated by E) and (ii) causes the transient to deviate from the behavior for simple positive feedback (shown as EC). $K = k_c a^2/D$.

It is important to note that the plateau currents in the i_T–$T^{-1/2}$ characteristics in Figure 4 are very close to the steady-state feedback values in the absence of kinetic complications,[3] and thus this portion of the SECM transient yields information on the tip–substrate distance (provided a is known). The range of dimensionless rate constant for which the transient may be utilized to provide information on the size of the gap can be defined by stipulating that, in order to be resolved experimentally, the plateau segment must prevail for at least 10% of the $T^{-1/2}$ "window" during which steady-state positive diffusional feedback is established for the kinetically uncomplicated case at the equivalent d/a. The start of this window is $(T = \infty)^{-1/2} = 0$, and inspection of the positive feedback data for $-1 \le \log (d/a) \le 0$ indicates that a suitable definition for the end of the window is $(2T_c)^{-1/2}$, a point at which (for all ratios of d/a considered) the feedback current is within 101% of the true steady-state value. The resulting kinetic zone in which the measurement of d/a from the transient is possible is illustrated in Figure 6, where it has been assumed that the plateau region will be sufficiently well-defined if the change in the current is less than 3% over the defined period. It is clear from Figure 6 that this method of measuring tip–substrate distance from the i_T–T characteristics applies to a wide range of kinetics.

Although only a single potential step is applied to the tip electrode, it should be recognized that SECM chronoamperometry is essentially equivalent to a *double*-step technique, since the direction of the tip electrode reaction is reversed on the substrate. A parallel can thus be drawn between this method and double-

(48) Shoup, D.; Szabo, A. *J. Electroanal. Chem. Interfacial Electrochem.* **1982**, *140*, 237.

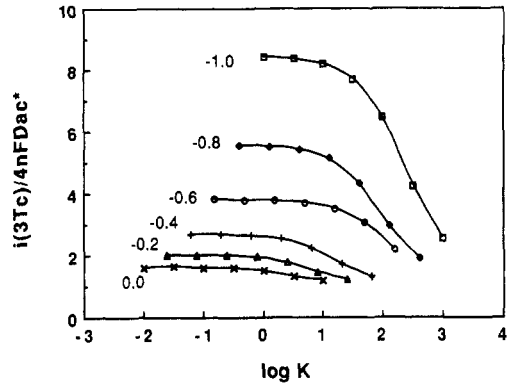

Figure 7. Working curves of $i_T(T_m=3T_c)$ vs K $(=k_c a^2/D)$. The numerical values on the curves denote log (d/a).

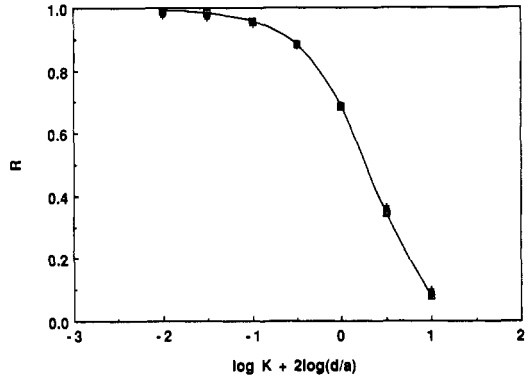

Figure 8. Universal working curve of the current ratio R as a function of $K(d/a)^2$. The points correspond to data derived from simulations for log (d/a) = −1.0 (□), −0.8 (○), −0.6 (×), and −0.4 (+).

potential-step chronoamperometry (DPSC) at a single electrode. In DPSC the ratio of currents measured at prescribed times on the forward and reverse steps is used to derive kinetic information.[17,49] Pursuing this analogy with SECM, a measurement time, T_m $(=t_m D/a^2)$, can be defined for the tip current. Inspection of the theoretical results suggests that, for the highest accuracy in the fast kinetic limit, a suitable value of T_m is around 3 times the critical time, T_c. Working curves of $i_T(T_m=3T_c)$ vs K for different ratios d/a, shown in Figure 7, show that minimizing the tip–substrate distance increases the magnitude of the rate constants accessible to measurement. A small tip–substrate separation also produces the greatest difference in the i_T values for the slow and fast kinetic limits and thus provides the most accurate means of measuring intermediate kinetics.

Since Figure 3 served to illustrate that the T_c–d/a characteristics for feedback SECM could essentially be derived by assuming one-dimensional diffusion (normal to the tip electrode), it follows that, if edge effects continue to be negligible at T_m, the tip current response should be independent of a, and depend upon d and k_c only. For this situation, the data in Figure 7 can be embodied in a universal working curve by defining the current difference ratio,

$$R = \frac{i_T(T_m)_K - i_T(T_m)_{K\to\infty}}{i_T(T_m)_{K=0} - i_T(T_m)_{K\to\infty}} \qquad (22)$$

and relating it to the quantity $K(d/a)^2$. The resulting curve is shown in Figure 8, from which it is evident that the assumption regarding the neglect of radial diffusion is valid to a very good approximation for log $(d/a) \leq -0.4$.

Steady-State Characteristics for the EC Mechanism. Although, in general, the advent of electrochemical methods involving microelectrodes has considerably reduced the period over which double-layer charging is significant in chronoamperometry (to the microsecond time scale[48]), problems may still arise with transient

(49) Andrieux, C. P.; Hapiot, P.; Savéant, J. M. *J. Phys. Chem.* **1988**, *92*, 5992.

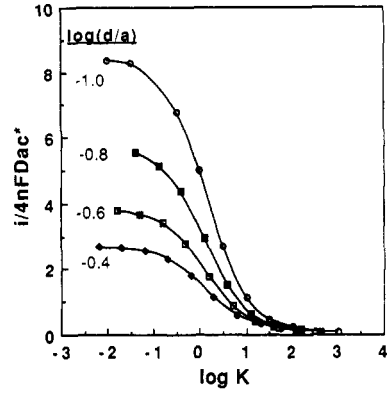

Figure 9. Steady-state i_T–K working curves for various values of log (d/a).

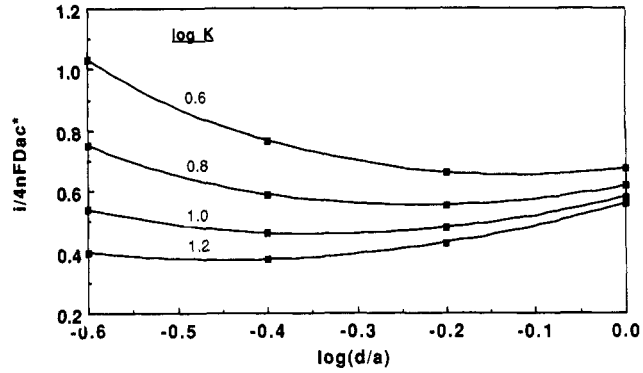

Figure 10. Steady-state tip current as a function of tip–substrate separation for various values of log K.

methods if additional faradaic surface processes compete on the time scale of the measurements. Such complications may be alleviated by making measurements under steady-state conditions. Moreover, steady-state currents can usually be measured with a better signal-to-noise ratio. The long-time limit to the calculated chronoamperometric data allows the deduction of steady-state i_T–K working curves for different ratios of d/a; typical plots are given in Figure 9. As expected, for a particular value of d/a, i_T reaches a maximum value in the limit of small K, while increasing K promotes a diminution in i_T until, in the limit of large K, the behavior is essentially equivalent to negative feedback from an insulating substrate. It is again clear that both the largest accessible rate constants and greatest accuracy, for kinetic determinations in the intermediate range, result from minimizing the tip–substrate distance.

Since steady-state SECM kinetic investigations involve measuring i_T as a function of the tip–substrate distance, with a single electrode of fixed radius, it is instructive to examine the overall form of the current–distance characteristics. For a wide range of K values, in the intermediate kinetic region, a minimum is observed in the i_T–d behavior. This arises because increasing d, on the one hand, leads to smaller fractions of O reaching the substrate for conversion to R (and subsequent feedback) but, on the other, increases the quantity of the species R diffusing into the gap. At small separations, the former process provides the dominant contribution to the trend in i_T, while the latter dominates at longer distances. The combined effect is thus an initial decrease in i_T with d and an increase in i_T at greater separations. The switch between the two effects occurs at closer tip–substrate separations, the larger the value of K, as illustrated in Figure 10. In principle, the position and magnitude of the minimum could be used to determine the value of K.

Inspection of the data in Figure 9 reveals that, to a reasonable approximation, the steady-state tip feedback current response is essentially analogous to that for an insulating substrate, i.e., $i_T < 1.1 i_t$(insulator), for

$$\log K > 1 - 2 \log (d/a) \qquad (23)$$

If this condition is satisfied then the steady-state current value provides a good indication of the ratio of (d/a).[3] Equation 23 and Figure 3, together, indicate that essentially pure positive or negative feedback behavior can be observed in the transient and steady-state modes, respectively, at some value of d/a in the range of practical interest, for virtually the full kinetic domain accessible to transient and steady-state measurements, and it should therefore be possible to extract information about d from these data.

Range of Measurable Rate Constants. It follows from the definition of K, eq 15, that the range of rate constants accessible to measurement by SECM feedback can, in principle, be varied over a very wide range by using electrodes with different radii, a. Probably of greatest interest is the estimation of the fastest chemical reaction which can be measured, which is governed by the smallest microdisk available and the closest distance to the substrate that it can be placed. Recent work[16] has demonstrated that submicrometer diameter ($a = 0.3$ μm) microdisk electrodes, suitable for quantitative SECM studies (i.e., compatible with the theoretical model outlined above) can be fabricated. With our current setup these can be positioned within a distance of several hundered nanometers to the substrate. It follows from the working curves presented above that rate constants in excess of 2×10^4 s^{-1} should be accessible from steady-state measurements with good accuracy. This is over an order of magnitude greater than the upper limit on measurable following chemical reaction rates from steady-state generation/collection experiments at the rotating ring-disk electrode[24] and far greater than the maximum which can be derived by using alternative "double electrodes" such as the paired microband electrode,[28] interdigitated array channel electrode,[27] and double-channel electrode.[26,50] The above limit on d with our present setup means that the fastest rate constant which may be measured by using potential step chronoamperometric SECM is currently of the same order as from steady-state measurements.

It should be noted that the fabrication of smaller ultramicrodisks and improvements in the closest distance to which they can be positioned to the substrate will lead to significant increases in the fastest rate constants accessible to the technique, since the upper limit on k_c is directly proportional to a^{-2}. In this context, we note that a method for manufacturing microdisk electrodes with radii in the range 5–36 nm has recently been reported,[51] and these may be suitable for quantitative SECM studies.

Experimental Section

Materials. All solutions were prepared with Milli-Q reagent water (Millipore Corp.). Solutions of DMPPD were obtained from the dichloride (Eastman Kodak, Rochester, NY). In order to avoid the oxidation of DMPPD by dissolved oxygen, these were made up by adding a known volume of 0.2 M DMPPD to a solution containing 0.25 M dipotassium hydrogen phosphate (Fisher Scientific, ACS certified) and 1 M potassium chloride (Baker Analyzed), which was rigorously deaerated with argon. The pH of the solution was adjusted to the approximate desired value through the addition of concentrated sodium hydroxide (Baker Analyzed) solution. The precise pH was measured with an Orion Research glass electrode and Model 701A meter. Ferrocyanide solutions contained approximately 1×10^{-3} M potassium ferrocyanide trihydrate (MCB Manufacturing Chemists, Inc.) and 1 M KCl.

Electrodes and Substrate. The SECM tip electrode was fabricated by sealing a 25-μm-diameter Pt wire in glass, as previously described.[1] After the electrode was polished to 0.25 μm, using a succession of finer diamond pastes (Buehler Ltd.), the glass surrounding the disk was fashioned into a cone by further polishing[1] to yield an electrode with an electrode/glass radius ratio, $RG = a/r_{glass}$, of 10 (measured optically). The electrode itself had a measured radius of 12.5 ± 0.5 μm, in excellent agreement with the nominal value. The effective radius was determined electrochemically by measurement of the diffusion-limited current for the oxidation of the aqueous ferrocyanide solution defined above. The diffusion coefficient under these conditions is 6.32×10^{-6} cm^2 s^{-1},[52] and application of eq 18 gave a value for a of 12.3 μm.

A silver wire (Goodfellows, Cambridge, UK) served as a quasi-reference electrode (AgQRE) in a two-electrode cell arrangement. A 0.5-in.-diameter quartz disk provided a suitable insulating substrate, and a similar disk was sputtered with platinum for experiments requiring a conductive substrate. The latter was unbiased, previous work[15] having established that its rest potential would be close to that required to reverse the direction of the tip electrode reaction at a rate close to the diffusion limit with the setup described here.

Procedure. The SECM apparatus has previously been described in detail.[1,2,5,6] A Teflon cell, equipped with a lid and a gas line for deaerating the solution with argon prior to making measurements, contained the AgQRE and substrate. The latter was secured flat in a recess cut into the base of the cell. The cell was attached to the X–Y stage, controlled by piezoelectric drivers (inchworms, 100 Å/s to 2 mm/s, Burleigh Instruments, Fischer, NY), while the tip was mounted on the z-piezoelectric inchworm. The apparatus was placed on an air table (Newport Research Corporation, Fountain Valley, CA) and shielded with a Faraday cage.

The tip potential was controlled by using a Model 175 programmer (Princeton Applied Research, NJ) and the current was measured with a homebuilt current follower.[4] Voltammograms were recorded directly on an X–Y recorder, and steady-state tip current–distance measurements were either measured on this device or, directly, using a high-impedance digital voltmeter. The potential step chronoamperometric characteristics were acquired with a Norland 3001A/DMX digital processing oscilloscope equipped a Model 3226B acquisition module (Norland Corp., Fort Atkinson, WI), with the current typically being recorded at 1-ms intervals. In order to compare the experimental transients with the theoretically simulated behavior, experimental data were uploaded to a DEC VAX 6410 mainframe computer via an IBM personal computer using a Kermit file-transfer program.

Several general procedures can be used for the measurement of tip–substrate distance, d:

(i) If half the substrate surface is conducting and half insulating, kinetic measurements can be made in the conducting region, and the tip translated at constant height to the insulating zone, where the resulting steady-state diffusion-limited current provides direct information on the tip–substrate distance.[3]

(ii) As discussed in the preceding section, for most of the kinetic domain accessible to measurement by feedback SECM, tip–substrate distance information can be extracted from either the transient or steady-state behavior.

(iii) An additional redox couple can be incorporated into the solution, which (a) does not interfere with the reaction of interest and (b) undergoes diffusion-limited positive feedback in a potential region where the reaction of interest does not occur. The steady-state tip current arising in the latter case is directly related to the tip–substrate distance.[3]

(iv) The SECM tip–substrate distance characteristics can be calibrated with reasonable accuracy as follows. The electrode is mounted with the same orientation on the z-piezoelectric inchworm and lowered until it makes contact with the substrate. Measurement of the diffusion-limited current for the electrolysis of a test species, which undergoes kinetically uncomplicated positive or negative feedback (with conducting or insulating substrates, respectively), then yields the distance of closest approach of the tip to the substrate,[3] and the calibrated z-piezoelectric device is used to provide subsequent separations relative to this position as the tip is backed away from the substrate. The validity of this procedure was confirmed by conducting several test experiments

(50) Aoki, K.; Tokuda, K.; Matsuda, H. *J. Electroanal. Chem. Interfacial Electrochem.* **1977**, *79*, 49.

(51) Casillas, N.; Snyder, S. R.; White, H. S. *J. Electrochem. Soc.* **1991**, *138*, 641.

(52) von Stackelberg, M.; Pilgram, M.; Toome, V. *Z. Elektrochem.* **1953**, *57*, 342.

against insulating and conducting substrates using, respectively, the oxidation of DMPPD (ca. pH 11) and ferrocyanide in aqueous solution. These experiments demonstrated that at the distance of closest approach the tip current was reproducible to within 10%, suggesting an error in the initial value of d of about this magnitude at the tip–substrate distances involved.[3]

For the experiments reported below on the oxidation of DMPPD, it was necessary to accumulate the data as rapidly as possible, because previous reports describe electrode filming by reaction products.[35] Method (iv) was therefore chosen for the measurement of the tip–substrate distance. Experiments involved initially placing the tip in contact with the surface and recording chronoamperometric characteristics and steady-state currents as a function of subsequent tip–substrate separations.

Experimental Results and Discussion

Preliminary Experiments. Steady-state voltammetry and potential-step chronoamperometry at a platinum ultramicrodisk electrode were used initially to investigate the oxidation of DMPPD (I) in basic aqueous solution (ca. pH 11). Previous work suggests that the overall reaction mechanism can be represented by the following scheme:[26,35]

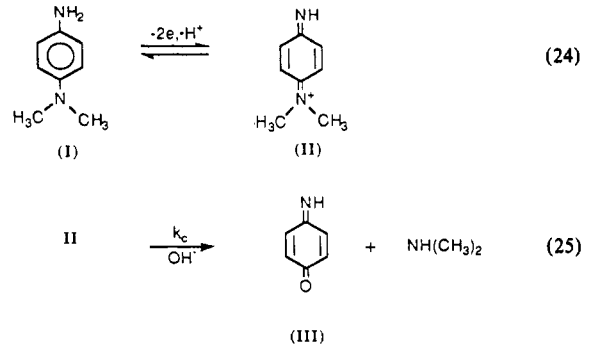

Although there are reports of problems arising from electrode filming by the products of the oxidation of this class of compounds,[53] and with this reaction in particular,[35] voltammetric studies indicated that provided the concentration of DMPPD was small (5×10^{-4} M) and the solution was rigorously deaerated from the time it was made up to the point of the measurements, stable diffusion-limited currents (attained at 0.40 V vs AgQRE) were maintained for periods of up to ca. 15 min. Limiting current measurements at pH 11.24, 10.78, and 10.20 yielded a diffusion coefficient of 7.2 (±0.1) $\times 10^{-6}$ cm^2 s^{-1} (via eq 18, using a = 12.3 μm), which is in good agreement with that of 6.8×10^{-6} cm^2 s^{-1} derived from rotating disk electrode voltammetry.[35] These two values for the two-electron-oxidation process are about 50% of the value of 1.19×10^{-5} cm^2 s^{-1} reported from channel electrode voltammetry.[26]

Potential-step chronoamperometric experiments were conducted by stepping the potential of the microdisk electrode from 0.00 V (where there are no faradaic processes) to 0.40 V vs AgQRE (where the oxidation of DMPPD is diffusion-controlled at this pH). For the concentration of DMPPD defined above, the resulting current transients were complicated by the fact that oxidation of the platinum electrode occurs in this potential region.[54] To circumvent this problem, the concentration of DMPPD was increased significantly in order to minimize the contribution to the total current arising from the oxidation of platinum. Figure 11 shows the chronoamperometric characteristics (plotted as $I(t)/I$(steady-state) vs $t^{-1/2}$) for (i) [DMPPD] = 15×10^{-3} M (pH = 11.24) and (ii) [DMPPD] = 8×10^{-3} M (pH = 7.80), along with the behavior predicted theoretically for a two-electron process at an ultramicrodisk electrode (eq 20) with $D = 7.2 \times 10^{-6}$ cm^2 s^{-1}. For almost all of the time range considered, there

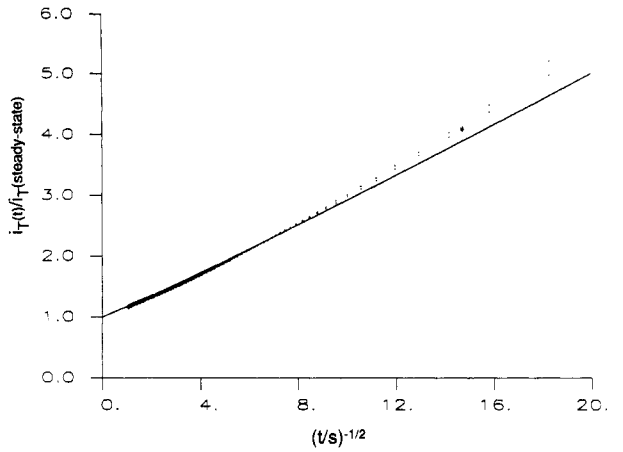

Figure 11. Potential-step chronoamperometric characteristics for the oxidation of DMPPD at a platinum ultramicrodisk electrode, a = 12.3 μm. The lower data points correspond to [DMPPD] = 15×10^{-3} M (pH 11.24) and the upper points to [DMPPD] = 8×10^{-3} M (pH 7.80). The solid line shows the theoretically predicted behavior for the two-electron process at an ultramicrodisk electrode, on the basis of eq 20, assuming $D = 7.2 \times 10^{-6}$ cm^2 s^{-1}.

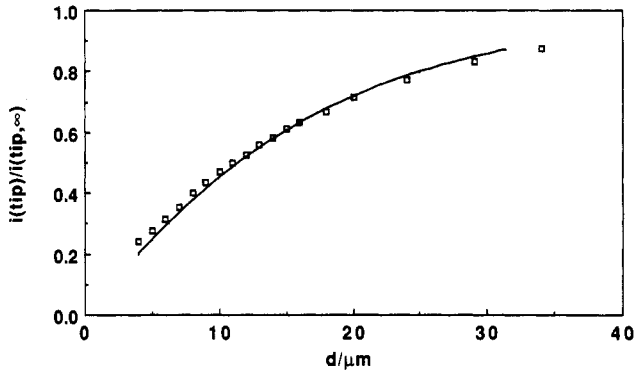

Figure 12. SECM steady-state i_T–d characteristics for the oxidation of DMPPD (5×10^{-4} M, pH 10.78) with a quartz substrate (□). The solid line shows the behavior predicted theoretically for an insulating substrate for an electrode with RG = 10.

is good agreement between theory and experiment. The currents measured at the shortest times are slightly larger than those expected theoretically, which is probably attributable to contributions from platinum oxidation. Several seconds after the establishment of a steady state, a diminution of i_T with time was observed, possibly indicating that filming of the electrode at the higher concentrations of DMPPD occurs more rapidly.

The results of these preliminary experiments suggested two strategies for measuring the rate of deamination of oxidized DMPPD via SECM feedback: steady-state current–distance measurements at low concentrations of DMPPD (5×10^{-4} M) and "single shot" transient measurements at a fixed tip–substrate distance with solutions containing high concentrations of DMPPD (around 10^{-2} M).

Steady-State i_T–d Measurements. To check the method for measuring tip–substrate distances, described above, initial feedback experiments were conducted on DMPPD oxidation, using an insulating quartz substrate. In this situation, the tip electrode reaction is defined by eq 24, the solution reaction by eq 25, and all species are assumed to be inert on the substrate surface. Typical experimental results, obtained at pH 11.24, are shown in Figure 12 along with the corresponding theoretical behavior for an electrode characterized by RG = 10.[3] Note that the following chemical reaction has no effect on the SECM i_T behavior, when an insulating substrate is used. The level of agreement between theory and experiment serves to vindicate method (iv) for making tip current–distance measurements, as described above.

The results of steady-state feedback experiments from a conducting platinum substrate for DMPPD (I) solutions of pH 10.20, 10.78, and 11.24 are shown in Figure 13, along with the theoretical

(53) Reed, R. C.; Wightman, R. M. In *Encyclopeadia of Electrochemistry of the Elements (Organic Section)*; Bard, A. J., Lund, H., Eds.; Marcel Dekker: New York, 1984; Vol. 15, p 1.

(54) Adams, R. N. *Electrochemistry at Solid Electrodes*; Marcel Dekker: New York, 1969; Chapter 7.

TABLE I: Definitions of the Terms in Eq A10

species	term	value
R, O	a^*_j $(1 \le j \le NE + NG - 1)$	$-\lambda_\rho(j)\left\{1 - \frac{\Delta\rho}{2}\left[1 + \frac{\exp(-ml\Delta\rho)}{s + m - m\exp(-ml\Delta\rho)}\right]\right\}$
R	b^*_j $(0 \le j \le NE + NG - 1)$	$1 + 2\lambda_\rho(j)$
O	b^*_j $(0 \le j \le NE + NG - 1)$	$1 + 2\lambda_\rho(j) + K\Delta T/2$
R, O	c^*_0	$-2\lambda_\rho(0)$
R, O	c^*_j $(1 \le j \le NE + NG - 2)$	$-\lambda_\rho(j)\left\{1 + \frac{\Delta\rho}{2}\left[1 + \frac{\exp(-ml\Delta\rho)}{s + m - m\exp(-ml\Delta\rho)}\right]\right\}$
R, O	d_j $(0 \le j \le NE + NG - 2)$	$\lambda_Z C_{j,k+1} + [1 - 2\lambda_Z]C_{j,k} + \lambda_Z C_{j,k-1}$
R	$d_{NE+NG-1}$	$\lambda_Z C_{NE+NG-1,k+1} + [1 - 2\lambda_Z]C_{NE+NG-1,k} + \lambda_Z C_{NE+NG-1,k-1} + \lambda_\rho(NE+NG-1)\left\{1 + \frac{\Delta\rho}{2}\left[1 + \frac{\exp(-ml\Delta\rho)}{s + m - m\exp(-ml\Delta\rho)}\right]\right\}$
O	$d_{NE+NG-1}$	$\lambda_Z C_{NE+NG-1,k+1} + [1 - 2\lambda_Z]C_{NE+NG-1,k} + \lambda_Z C_{NE+NG-1,k-1}$

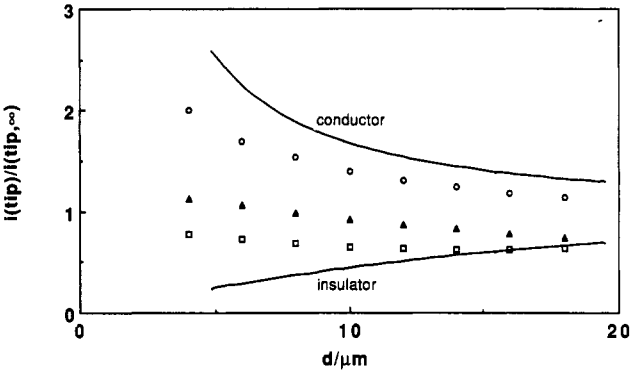

Figure 13. SECM steady-state i_T–d characteristics for the oxidation of DMPPD (5×10^{-4} M), at pH 10.20 (○), 10.78 (△), and 11.24 (□), with an unbiased platinum substrate. The solid lines represent theoretical behavior in the absence of coupled reaction for insulating and conductive substrates.

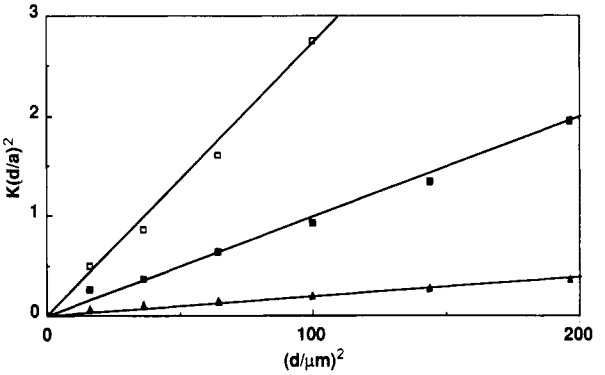

Figure 14. Kinetic analysis of the data in Figure 13 [pH 10.20 (▲), pH 10.78 (■), pH 11.24 (□)] following conversion of the current data to values of K via working curves.

behavior for positive and negative feedback from conducting and insulating substrates. The tip electrode reaction is again as defined above, while the reaction in eq 26 should occur on the substrate:

$$II + 2e + H^+ \rightarrow I \qquad (26)$$

For a particular tip–substrate distance, the feedback current decreases as the pH increases, since this promotes the consumption of II via the deamination reaction, eq 25. The normalized tip currents in Figure 13 were converted to their kinetic equivalents, K, via $i_T/i_{T,\infty}$–K working curves generated for each value of d/a. It follows from the definition of K (eq 15) that a plot of $K(d/a)^2$ vs d^2 for the data at each pH should be linear and intersect the origin, with the slope yielding a value for the ratio k_c/D. Figure 14 shows that all three sets of data analyze satisfactorily on this basis. Application of the diffusion coefficient for DMPPD defined above yields values for k_c of 19 (pH 11.24), 5.8 (pH 10.78), and 1.4 (pH 10.20) s^{-1}. The corresponding values for the second-order rate constant, $k_2 = k_c/[OH^-]$, were found to be reasonably consistent: 1.1×10^4, 9.5×10^3, and 9.0×10^3 mol^{-1} dm^3 s^{-1}, respectively. The average value of k_2 is lower than that measured spectrophotometrically,[42] but there is a significant difference in the ionic strengths of the solutions employed in the two studies. The average value of k_2 is also lower than the rate constant of $(1.8 \pm 0.2) \times 10^4$ mol^{-1} dm^3 s^{-1} obtained from double-channel electrode collection efficiency measurements under identical solution conditions. However, in the latter case, the diffusion coefficient used in calculating the rate constant was twice as large as that measured here. If the value of D determined from both this study and rotating disk electrode voltammetry is used, the value of k_2 is found to be closer to that determined above.

Chronoamperometry. Experiments were carried out with [DMPPD] = 8.0×10^{-3} M (pH 7.80) and 15×10^{-3} M (at all other pH), for the reasons outlined above, dictating that only

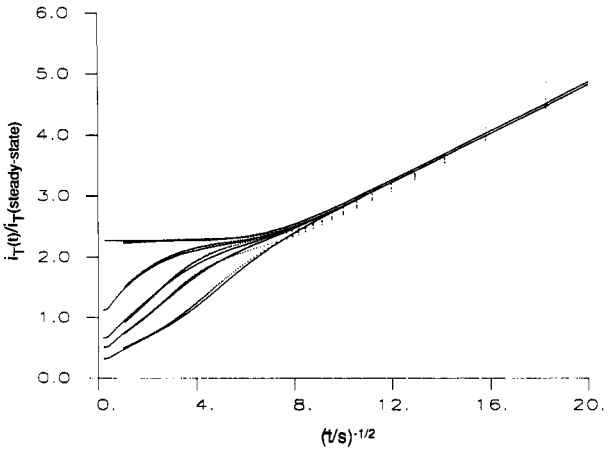

Figure 15. Experimental potential-step chronoamperometric characteristics (···) for the oxidation of DMPPD at pH 7.80 (upper curve), pH 10.90, pH 11.38, pH 11.63, and pH 12.42 (lowest curve). The solid lines show the corresponding behavior predicted theoretically for each pH using values for k_c derived from the steady-state feedback results.

"single shot" experiments were possible. Figure 15 shows chronoamperometric data, plotted as a function of the inverse square root of time, obtained at pH 7.80, 10.90, 11.38, 11.63, and 12.42 with an approximate tip–substrate distance of 6.5 μm, as deduced from the plateau regions of the data at pH 7.80 (where the contribution from the homogeneous chemical reaction is negligible) and pH 10.90 and 11.38. For comparison with the experimental results, theoretical curves showing the behavior expected by using the average rate constant derived from the steady-state results are also given. These correspond to k_c = 7.8 (pH 10.90), 24 (pH 11.38), 42 (pH 11.63), and 260 (pH 12.42) s^{-1}, while for the pH 7.80 data the deamination process was assumed to proceed to a

TABLE II: Definitions of the Terms in Eq A11[a]

species	term	radial domain	value
R, O	a^{**}_k $(2 \le k \le NZ - 1)$	$0 \le j \le NE + NG - 1$	$-\lambda_Z$
R	b^{**}_1	$0 \le j \le NE$	$1 + 2\lambda_Z$
		$NE + 1 \le j \le NE + NG - 1$	$1 + \lambda_Z$
O	b^{**}_1	$0 \le j \le NE + NG - 1$	$1 + \lambda_Z$
R, O	b^{**}_k $(2 \le k \le NZ - 2)$	$0 \le j \le NE + NG - 1$	$1 + 2\lambda_Z$
R	b^{**}_{NZ-1}	$0 \le j \le NE + NG - 1$	$1 + \lambda_Z$
O	b^{**}_{NZ-1}	$0 \le j \le NE + NG - 1$	$1 + 2\lambda_Z$
R, O	c^{**}_k $(1 \le k \le NZ - 2)$	$0 \le j \le NE + NG - 1$	$-\lambda_Z$
R	d^{*}_k $(1 \le k \le NZ - 2)$	$j = 0$	$\{1 - 2\lambda_\rho(0)\}C^*_{0,k} + 2\lambda_\rho(0)C^*_{1,k}$
R	d^{*}_1	$1 \le j \le NE + NG - 1$	rhs[b] of eq A9
O	d^{*}_1	$j = 0$	$\{1 - 2\lambda_\rho(0) - K\Delta T/2\}CO^*_{0,1} + 2\lambda_\rho(0)CO^*_{1,1} + \lambda_Z CR^{**}_{0,1}$
O	d^{*}_k $(2 \le k \le NZ - 2)$	$j = 0$	$\{1 - 2\lambda_\rho(0) - K\Delta T/2\}C^*_{0,k} + 2\lambda_\rho(0)C^*_{1,k}$
O	d^{*}_1	$1 \le j \le NE$	rhs eq A9 $+ \lambda_Z CR^{**}_{j,1}$
O	d^{*}_1	$NE + 1 \le j \le NE + NG - 1$	rhs eq A9
R, O	d^{*}_k $(2 \le k \le NZ - 2)$	$1 \le j \le NE + NG - 1$	rhs eq A9
R	d^{*}_{NZ-1}	$j = 0$	$\{1 - 2\lambda_\rho(0)\}CR^*_{0,NZ-1} + 2\lambda_\rho(0)CR^*_{1,NZ-1} + \lambda_Z CO^{**}_{0,NZ-1}$
R	d^{*}_{NZ-1}	$1 \le j \le NE + NG - 1$	rhs eq A9 $+ \lambda_Z CO^{**}_{j,NZ-1}$
O	d^{*}_{NZ-1}	$j = 0$	$\{1 - 2\lambda_\rho(0) - K\Delta T/2\}C^*_{0,NZ-1} + 2\lambda_\rho(0)C^*_{1,NZ-1}$
O	d^{*}_{NZ-1}	$1 \le j \le NE + NG - 1$	rhs eq A9

[a] Note: In the expression for the d^*_k term, $C_{j,k}$ refers to either R or O, identified in the first column of the table. When the d^*_k term involves the concentrations of both R and O, these are denoted by $CR_{j,k}$ and $CO_{j,k}$, respectively. [b] Right-hand side.

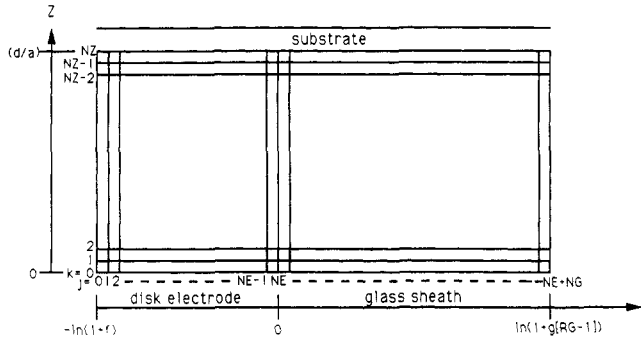

Figure 16. SECM finite-difference mesh for the ADI method calculations.

negligible extent. Reasonably good agreement between theory and experiment is observed for all pH, particularly given the experimental difficulties associated with electrode filming under these particular conditions. Even with the relatively large microelectrode and tip–substrate distances employed here, it is clear that the transient method is both sensitive to the rate of the following chemical reaction over a wide dynamic range (almost 2 orders of magnitude in k_c) and can be used to probe relatively fast following chemical kinetics.

Conclusions

This study has demonstrated that steady-state and chronoamperometric feedback measurements at the SECM are useful new approaches to the problem of measuring the kinetics of following homogeneous chemical reactions involved in electrode processes. Although, by way of example, the E_rC_i mechanism has been considered in this paper, it should be noted that feedback SECM could be used to study other mechanisms involving either alternative classes of following chemical reactions (e.g., second-order processes), intermediate/sandwiched chemical processes (e.g., in the ECE/DISP scheme), or parallel (catalytic) homogeneous reactions coupled to reversible electron transfer. The ADI numerical model developed in this paper could readily be adapted to cover these additional cases.

With the present SECM technology, first-order rate constants in excess of 2×10^4 s^{-1} should be accessible to measurement under steady-state conditions, which surpasses the upper limits on measurable rate constants attainable from steady-state collection efficiency measurements at alternative electrode geometries, such as the rotating ring-disk,[24] double-channel,[26] interdigitated channel array,[27] or paired microband[28] electrodes. Moreover, practical reductions in the size of both the tip electrode and the tip–substrate distance will greatly expand the magnitude of the kinetic domain accessible to the technique. Work is currently in progress in this group on these practical aspects of SECM, and initial results in the area appear promising.

Acknowledgment. We gratefully acknowledge the support of this research by the Texas Advanced Research Program and the National Science Foundation (CHE 8901450). P.R.U. thanks SERC for the award of a NATO Fellowship. We thank Drs. G. Denault, D. T. Pierce, and D. O. Wipf for useful discussions.

Appendix

In order to effect an efficient numerical solution to the SECM feedback problem, the Z and R variables were transformed with functions which reflected the predicted (steady-state) concentration profiles.[55,56] For the radial direction, appropriate functions are

$$\rho = -\ln(1 + f[1 - R]) \qquad (0 \le R \le 1) \qquad \text{(A1)}$$

$$\rho = \ln(1 + g[R - 1]) \qquad (1 < R \le RG) \qquad \text{(A2)}$$

where f and g are constants (with values specified below). A priori predictions of the concentration profiles for R and O in the Z direction are difficult, since they vary dramatically with the magnitude of the rate constant, K, and the ratio d/a. The Z coordinate was therefore untransformed, which is the best choice for a conducting substrate, in the absence of kinetic complications, based upon the concentration profiles for the analogous situation in a dual electrode TLC.[57] For the calculation of the feedback current over an insulator, the following function was introduced

$$\zeta = \ln(1 + hZ) \qquad \text{(A3)}$$

where h is a constant (typically in the range 1–5). In this Appendix we will consider the development for the EC case (over a conductor) only, the modifications to other cases should be self-evident.

Introduction of eqs 11–15, A1, and A2 into eqs 3 and 4 yields the following diffusion equations for species A and B

(55) Joslin, T.; Pletcher, D. *J. Electroanal. Chem. Interfacial Electrochem.* **1974**, *49*, 172.

(56) Feldberg, S. W. *J. Electroanal. Chem. Interfacial Electrochem.* **1981**, *127*, 1.

(57) Hubbard, A. T.; Anson, F. C. In *Electroanalytical Chemistry*; Bard, A. J., Ed.; Marcel Dekker: New York, 1970; Vol. 4, p 129.

$$\frac{\partial C_A}{\partial T} = s^2 \exp(2m\rho)\frac{\partial^2 C_A}{\partial \rho^2} + \left[\frac{s^2 \exp(m\rho)}{s - m\exp(-m\rho) + m} + ms^2 \exp(2m\rho)\right]\frac{\partial C_A}{\partial \rho} + \frac{\partial^2 C_A}{\partial Z^2} \quad (A4)$$

$$\frac{\partial C_B}{\partial T} = s^2 \exp(2m\rho)\frac{\partial^2 C_B}{\partial \rho^2} + \left[\frac{s^2 \exp(m\rho)}{s - m\exp(-m\rho) + m} + ms^2 \exp(2m\rho)\right]\frac{\partial C_B}{\partial \rho} + \frac{\partial^2 C_B}{\partial Z^2} - KC_B \quad (A5)$$

where $m = 1$ and $s = f$ $(0 \le R \le 1)$; $m = -1$ and $s = g$ $(1 < R \le RG)$. The modifications to the boundary conditions should be evident.

The mesh and notation for the finite-difference calculations are shown in Figure 16. Points in the R and Z directions are clearly denoted by j and k, respectively. The number of points in the radial direction over the electrode and glass sheath, NE and {NG − NE}, respectively, was typically 80. At least 100 points were used in the Z direction, which ensured that there were always a sufficient number of points covering the size of the estimated reaction layer (eq 21) with the values of K considered here. The separations between grid points in the radial and Z direction are denoted by

$$\Delta\rho = \ln(1 + f)/NE \quad \text{(electrode vicinity)}$$

$$\Delta\rho = \ln(1 + g[RG - 1])/\{NG - NE\} \quad \text{(insulating sheath)}$$

$$\Delta Z = (d/a)/NZ$$

The basis of the ADI method is to utilize two finite-difference equations which, considering the calculation over an interval T to $T + \Delta T$, are employed over successive half time steps of $\Delta T/2$. The derivatives in eqs A4 and A5 are replaced by finite-difference equivalents, formulated for the first equation in terms of known concentration values in the Z direction and unknowns in the ρ direction and vice versa for the second equation. The equation for the first time step is of the form

$$\frac{C^*_{j,k} - C_{j,k}}{(\Delta T/2)} = \frac{s^2 \exp(2ml\Delta\rho)}{(\Delta\rho)^2}[C^*_{j+1,k} - 2C^*_{j,k} + C^*_{j-1,k}] + \left[\frac{s^2 \exp(ml\Delta\rho)}{s - m\exp(-ml\Delta\rho) + m} + s^2 \exp(2ml\Delta\rho)\right] \times \left[\frac{C^*_{j+1,k} - C^*_{j-1,k}}{2(\Delta\rho)}\right] + \frac{C_{j,k+1} - 2C_{j,k} + C_{j,k-1}}{(\Delta Z)^2} - qKC^*_{j,k} \quad (A6)$$

where $C_{j,k}$ denotes the (normalized) concentration of either A or B at point j,k, the integer $l = NE - j$ in the vicinity of the electrode, while $l = j - NE$ in the domain of the glass sheath. When $C_{j,k}$ denotes A, $q = 0$, while $q = 1$ for B. An asterisk on the quantity $C_{j,k}$ identifies those concentrations which are to be evaluated at the (new) time, $T + \Delta T/2$, from known (old) concentrations evolved at the previous time, T. For the second time step the equation is

$$\frac{C^{**}_{j,k} - C^*_{j,k}}{(\Delta T/2)} = \frac{s^2 \exp(2ml\Delta\rho)}{(\Delta\rho)^2}[C^*_{j+1,k} - 2C^*_{j,k} + C^*_{j-1,k}] + \left[\frac{s^2 \exp(ml\Delta\rho)}{s - m\exp(-ml\Delta\rho) + m} + s^2 \exp(2ml\Delta\rho)\right] \times \left[\frac{C^*_{j+1,k} - C^*_{j-1,k}}{2(\Delta\rho)}\right] + \frac{C^{**}_{j,k+1} - 2C^{**}_{j,k} + C^{**}_{j,k-1}}{(\Delta Z)^2} - qKC^*_{j,k} \quad (A7)$$

$C^{**}_{j,k}$ are now the new concentrations to be calculated from $C^*_{j,k}$ (the old). Notice that with this formulation the kinetic term is centered at the midpoint of the overall time step, ΔT.

The calculation in the radial direction employs eq A1 for ρ, in the vicinity of the electrode, up to $j = NE$ (and thus includes the concentration at the point $j = NE + 1$). For specified values of NE and NG, the parameters f and g in eqs A1 and A2 are therefore interdependent, in order to ensure a match between the electrode and glass grids at this point (in R space) and at $R = 1$ ($\rho = 0$). In computational practice NE and NG were predefined and a value of f was selected (typically in the range 2–10) from which the corresponding value of g, required to satisfy the above condition, was calculated.

Since eq A6 is implicit in the ρ direction and eq A7 is implicit in the Z direction, the overall procedure is stable for any size time step.[39-41] This is of great advantage in the problem considered here where the concentration changes are rapid at short times (necessitating small ΔT for an accurate simulation) and more gradual at longer times, where larger time steps can thus be utilized. It should be noted that an explicit finite-difference simulation of this problem would be prohibitive in terms of computer time, given the restriction on the magnitude of ΔT[40,41] imposed to retain stability with this method.

For the calculation, eqs A6 and A7 are rearranged to

$$-\lambda_\rho(j)\left\{1 - \frac{\Delta\rho}{2}\left[1 + \frac{\exp(-ml\Delta\rho)}{s + m - m\exp(-ml\Delta\rho)}\right]\right\}C^*_{j-1,k} + [1 + 2\lambda_\rho(j) + qK\Delta T/2]C^*_{j,k} - \lambda_\rho(j)\left\{1 + \frac{\Delta\rho}{2}\left[1 + \frac{\exp(-ml\Delta\rho)}{s + m - m\exp(-ml\Delta\rho)}\right]\right\}C^*_{j+1,k} = \lambda_Z C_{j,k+1} + [1 - 2\lambda_Z]C_{j,k} + \lambda_Z C_{j,k-1} \quad (A8)$$

$$-\lambda_Z C^{**}_{j,k-1} + [1 + 2\lambda_Z]C^{**}_{j,k} - \lambda_Z C^{**}_{j,k+1} = \lambda_\rho(j)\left\{1 - \frac{\Delta\rho}{2}\left[1 + \frac{\exp(-ml\Delta\rho)}{s + m - m\exp(-ml\Delta\rho)}\right]\right\}C^*_{j-1,k} + [1 - 2\lambda_\rho(j) - qK\Delta T/2]C^*_{j,k} + \lambda_\rho(j)\left\{1 + \frac{\Delta\rho}{2}\left[1 + \frac{\exp(-ml\Delta\rho)}{s + m - m\exp(-ml\Delta\rho)}\right]\right\}C^*_{j+1,k} \quad (A9)$$

where

$$\lambda_\rho(j) = \frac{(\Delta T/2)s^2 \exp(2ml\Delta\rho)}{(\Delta\rho)^2}$$

$$\lambda_Z = (\Delta T/2)/(\Delta Z)^2$$

Two-point approximations of the derivative boundary conditions at $Z = 0$, $1 < R \le RG$ and $Z = d/a$, $0 \le R \le RG$ were considered to be sufficient to give the level of accuracy required here. The condition at $R = 0$, $0 < Z < d/a$ was handled by using the symmetry about this boundary. Application of the boundary conditions condenses the calculation in the radial direction (eq A8) to {NE + NG} simultaneous equations in {NE + NG} unknowns for each row (i.e., a total of NZ − 1 sets of equations):

$$\left.\begin{aligned} b^*_0 C^*_0 + c^*_0 C^*_1 &= d_0 \\ a^*_j C^*_{j-1} + b^*_j C^*_j + c^*_j C^*_{j+1} &= d_j \} \quad (1 \le j \le NE + NG - 2) \\ a^*_{NE+NG-1} C^*_{NE+NG-2} + b^*_{NE+NG-1} C^*_{NE+NG-1} &= d_{NE+NG-1} \end{aligned}\right\}$$

$$(1 \le k \le NZ - 1) \quad (A10)$$

Identities for each of the terms in eq A10 for O and R are given in Table I. The initial condition (eq 5) supplies the first set of values for the vector $\{\mathbf{d}\}_{0 \le j \le NE+NG-1}$ along each row, from which the corresponding values of $C^*_{0 \le j \le NE+NG-1,k}$ can be calculated. Since eq A10 is a tridiagonal matrix equation, the Thomas algorithm[40,41,58] was used to provide an efficient method of solution.

(58) Thomas, L. H. *Watson Sci. Comput. Lab. Rep.*; Columbia University, New York, 1949.

The calculation in the Z direction, after application of the boundary conditions to eq A9, is of the form

$$\left.\begin{aligned} b^{**}_1C^{**}_1 + c^{**}_1C^{**}_2 &= d^*_1 \\ a^{**}_kC^{**}_{k-1} + b^{**}_kC^{**}_k + c^{**}_kC^{**}_{k+1} &= d^{**}_k \quad (2 \le k \le N-2) \\ a^{**}_{NZ-1}C^{**}_{NZ-2} + b^{**}_{NZ-1}C^{**}_{NZ-1} &= d^*_{NZ-1} \end{aligned}\right\}$$
$$(0 \le j \le NE + NG - 1) \quad (A11)$$

where each of the terms are defined in Table II. The values for the vector $\{\mathbf{d}^*\}_{1\le k\le NZ-1}$ for each column are calculated from the corresponding $C^*_{j,k}$ values evaluated at the previous half-time step. Values of $C^{**}_{j,k}$ are then calculated along each column, starting at the $R = 0$ boundary and working across to the radial edge of the glass sheath. The calculation starts with species R followed by O for all k at each value of j. It is apparent from Table II that the calculation of $CR^{**}_{j,k}$ (for each column in the range $0 \le j \le NE$) requires a knowledge of $CO^{**}_{j,NZ-1}$, which remains to be calculated. This problem was circumvented by adopting an iterative procedure in which, for a particular column, $CO^{**}_{j,NZ-1}$ was initially approximated by $CO^*_{j,NZ-1}$ followed by successive calculations of $CR^{**}_{j,k}$ and $CO^{**}_{j,k}$, using the newly determined value for $CO^{**}_{j,NZ-1}$ at each iteration, until the values of $CR^{**}_{j,NZ-1}$ and $CO^{**}_{j,NZ-1}$ were unchanged (to within 0.01%) upon further iteration. The validity of this procedure was checked by calculating the current-time characteristics for feedback from a conductor in a similar fashion, and comparing the results to those obtained by invoking the concept of mass conservation (since $D_O = D_R$), and solving the equivalent "one species" case (which avoids the above-mentioned problem).

At the end of the second half-time step, the current at the disk electrode was evaluated by the summation of the local fluxes in the normal direction. A five-point finite-difference approximation for the flux was used, as recommended by other workers.[59] The calculation then proceeds to the next time step, with the values for $\{\mathbf{d}\}_{0\le j\le NE+NG-1}$ along each row formulated from the appropriate $C^{**}_{j,k}$.

The above formulation was coded in Fortran in double precision, and the program was executed on a DEC VAX 6410 mainframe computer. The length of time required to evaluate a full current transient depended upon the number of grid points employed, the value of the ratio d/a and the size of K. By optimization of the size of the time step throughout the calculation, only 5-10 min were typically required to determine the characteristics up to $T = 130$ (equivalent to the steady state for the case of RG = 10 considered here). Even for the worst case, no more than about 30-40 min of CPU time was required.

Registry No. Pt, 7440-06-4; *N,N*-dimethyl-*p*-phenylenediamine, 99-98-9.

(59) Britz, D. *Anal. Chim. Acta* **1987**, *19*, 277.

Absorption Effects in Laser Desorption of Neutral Organic Molecules

Gary R. Kinsel, Josef Lindner, Jürgen Grotemeyer,* and Edward W. Schlag

Institut für Physikalische und Theoretische Chemie der Technischen Universität München, Lichtenbergstrasse 4, D-8046 Garching, Germany *(Received: February 14, 1991)*

Resonant vs nonresonant laser desorption of neutral molecules was investigated by laser desorbing a variety of compounds at the four harmonic wavelengths of a Nd:YAG laser (266, 355, 532, and 1064 nm) and subsequently ionizing the jet-entrained neutrals with 255-nm multiphoton ionization. The compounds investigated exhibited a spectrum of absorption and thermal stability characteristics and a mass range up to 2000 Da. Nonresonant laser desorption required significantly higher desorbing laser powers and did not produce detectable intact neutral molecular species from the larger, more thermally labile compounds. Resonant laser desorption of neutrals efficiently produced abundant intact molecular species at low laser powers by coupling the desorbing laser energy directly into the sample bulk. All compounds investigated under resonant laser desorption conditions gave abundant postionized molecular ion signals. The results of these investigations are presented and discussed with respect to previous investigations of direct laser desorption of ions.

Introduction

In the past several years this research group has demonstrated the analytical potential of infrared laser desorption (LD) of neutral molecules at the CO_2 wavelength (10.6 μm) coupled with multiphoton ionization (MUPI) reflectron time-of-flight mass spectrometry (RETOF-MS) for the analysis of a wide variety of molecules of biological and practical interest.[1-3] Most recently protected mono- and dinucleotides have been successfully analyzed by use of this technique.[4,5] Several other research groups have also presented results using a similar approach where LD of neutral molecules is followed by a separate ionization step.[6-8]

In principle, the advantage of separating the LD step from the ionization step is that each step can be independently optimized to yield improvements in system performance while allowing greater flexibility in both ionization and desorption conditions. In addition, neutral emission during low-power LD may be several orders of magnitude greater than ion emission which may allow gains in the sensitivity of the decoupled approach as compared to direct LD of ions.[9] Finally, postionization of desorbed neutrals allows the high-resolution capacity of the RETOF-MS to be realized independent of the specific neutral formation conditions.

* Address correspondence to this author.

(1) Grotemeyer, J.; Walter, K.; Boesl, U.; Schlag, E. W. *Org. Mass Spectrom.* **1986**, *21*, 595.
(2) Grotemeyer, J.; Walter, K.; Boesl, U.; Schlag, E. W. *Org. Mass Spectrom.* **1986**, *21*, 645.
(3) Grotemeyer, J.; Walter, K.; Boesl, U.; Schlag, E. W. *Int. J. Mass Spectrom. Ion Proc.* **1987**, *78*, 69.
(4) Lindner, J.; Grotemeyer, J.; Schlag, E. W. *Int. J. Mass Spectrom. Ion Proc.* **1990**, *100*, 267.
(5) Lindner, J.; Grotemeyer, J.; Schlag, E. W. *J. Mol. Struct.* **1991**, submitted for publication.
(6) Engelke, F.; Hahn, J. H.; Henke, W.; Zare, R. *Anal. Chem.* **1987**, *59*, 909.
(7) Li, L.; Lubman, D. M. *Rev. Sci. Instrum.* **1988**, *59*, 557.
(8) Frey, R.; Holle, A.; Weiss, G.; Franzen, J.; Koch, D. *Proceedings of the 36th Annual Conference on Mass Spectrometry and Allied Topics*, San Francisco, CA, June 1988; p 185.
(9) van Breeman, R. B.; Snow, M.; Cotter, R. J. *Int. J. Mass Spectrom. Ion Phys.* **1983**, *49*, 35.

0022-3654/91/2095-7824$02.50/0